AIP | The Journal of Chemical Physics

A nanosecond pulsed laser heating system for studying liquid and supercooled liquid films in ultrahigh vacuum

Yuntao Xu, Collin J. Dibble, Nikolay G. Petrik, R. Scott Smith, Alan G. Joly, Russell G. Tonkyn, Bruce D. Kay, and Greg A. Kimmel

Citation: The Journal of Chemical Physics **144**, 164201 (2016); doi: 10.1063/1.4947304
View online: http://dx.doi.org/10.1063/1.4947304
View Table of Contents: http://scitation.aip.org/content/aip/journal/jcp/144/16?ver=pdfcov
Published by the AIP Publishing

A nanosecond pulsed laser heating system for studying liquid and supercooled liquid films in ultrahigh vacuum

Yuntao Xu,[a] Collin J. Dibble,[a] Nikolay G. Petrik, R. Scott Smith, Alan G. Joly, Russell G. Tonkyn, Bruce D. Kay,[b] and Greg A. Kimmel[b]
Physical Sciences Division, Pacific Northwest National Laboratory, P.O. Box 999, Richland, Washington 99352, USA

(Received 29 January 2016; accepted 8 April 2016; published online 26 April 2016)

A pulsed laser heating system has been developed that enables investigations of the dynamics and kinetics of nanoscale liquid films and liquid/solid interfaces on the nanosecond time scale in ultrahigh vacuum (UHV). Details of the design, implementation, and characterization of a nanosecond pulsed laser system for transiently heating nanoscale films are described. Nanosecond pulses from a Nd:YAG laser are used to rapidly heat thin films of adsorbed water or other volatile materials on a clean, well-characterized Pt(111) crystal in UHV. Heating rates of $\sim 10^{10}$ K/s for temperature increases of ~100–200 K are obtained. Subsequent rapid cooling ($\sim 5 \times 10^9$ K/s) quenches the film, permitting *in-situ*, post-heating analysis using a variety of surface science techniques. Lateral variations in the laser pulse energy are ~±2.7% leading to a temperature uncertainty of ~±4.4 K for a temperature jump of 200 K. Initial experiments with the apparatus demonstrate that crystalline ice films initially held at 90 K can be rapidly transformed into liquid water films with T > 273 K. No discernable recrystallization occurs during the rapid cooling back to cryogenic temperatures. In contrast, amorphous solid water films heated below the melting point rapidly crystallize. The nanosecond pulsed laser heating system can prepare nanoscale liquid and supercooled liquid films that persist for nanoseconds per heat pulse in an UHV environment, enabling experimental studies of a wide range of phenomena in liquids and at liquid/solid interfaces. *Published by AIP Publishing.* [http://dx.doi.org/10.1063/1.4947304]

I. INTRODUCTION

Liquid/solid interfaces, such as those in living organisms,[1] photoelectrochemical cells,[2–4] photocatalysts,[5–7] nuclear reactors,[8] and nuclear waste depositories,[8] are ubiquitous both in nature and technology. Despite their importance, a molecular-level understanding of such systems is lacking due to numerous experimental and theoretical challenges. For example, details of the growth mode and wetting properties of very thin—from one to several tens of monolayers (MLs) thick—crystalline ice (CI) and amorphous solid water (ASW) films at cryogenic temperatures have been determined for several well-characterized substrates including some metal single crystals, graphene, and some metal oxides.[9–19] Ultrahigh vacuum (UHV) surface science techniques, such as infrared reflection absorption spectroscopy (IRAS) and temperature programmed desorption spectroscopy (TPD), coupled with theory, have proved to be useful for elucidating such structures and dynamics. In contrast, relatively little experimental information is available for the molecular-level structure and dynamics of comparably thin liquid water films on surfaces.[19–25] Therefore, experimental approaches that permit the creation and study of thin liquid water films are needed.

Typically, the high vapor pressure of liquid water and other volatile materials leads to rapid desorption of nanoscale films in UHV, limiting their ability to be studied in that environment. To circumvent this problem, vapor deposition on a substrate at low temperature (below the glass transition) has been used to "freeze" the liquid as an amorphous solid. For example, water films created at low temperatures (<130 K) by vapor deposition have the mechanical properties of a solid but the molecular structure of a liquid. When water is deposited under these conditions the resulting material is called amorphous solid water (ASW).[26] The same technique can be used to create a wide variety of amorphous solids. The amorphous film can then be heated above the "glass transition" temperature where the film transforms into a supercooled liquid, albeit one in which the molecular motions are 10^{15} times slower than a liquid at room temperature.[27] The combination of slow molecular motion and the nanoscale thickness of the films has been used to measure the diffusivity of deeply supercooled liquid water in the range of $\sim 1 \times 10^{-15}$ to $\sim 1 \times 10^{-12}$ cm^2/s from 150 to 160 K.[28,29] Unfortunately, at the heating rates used in those experiments (~1 K/s), ASW rapidly transforms to crystalline ice, which limits the upper measurement temperature to about 160 K. Additionally, the films undergo rapid evaporation (sublimation) above 140 K. Because rapid crystallization limits the ability to probe the properties of supercooled liquid water above ~160 K and below ~230 K, this temperature region is referred to as "no-man's land."[30]

[a]Y. Xu and C. J. Dibble contributed equally to this work.
[b]Authors to whom correspondence should be addressed. Electronic addresses: gregory.kimmel@pnnl.gov and bruce.kay@pnnl.gov

Attempts to enter "no-man's land," either by heating the amorphous solid or supercooling from the liquid phase, are challenging. Experimental approaches from the low temperature side require rapid heating of an amorphous solid to circumvent the rapid crystallization kinetics. For example, Sadtchenko *et al.* have developed an ultrafast microcalorimetric method in which a 10 μm wire is used as a substrate for the deposition of amorphous solids. The wire can be heated at rates of 10^5 K/s and changes in the resistivity are used to measure the heat capacity of the amorphous material as a function of temperature.[31,32] Other approaches to rapidly heat nanoscale ASW films include laser-induced injections of hot electrons from the underlying Pt(111) substrate[33] and direct heating of the ASW layer itself using nanosecond laser pulses of infrared radiation at 3424 cm^{-1}.[34] In both of these cases, large amounts of the film were ablated with each laser pulse. On the other hand, attempts to enter "no-man's land" from the high-temperature side require rapid cooling of liquid or gas phase water. One approach uses liquid jets where a micron-sized diameter jet is sprayed into vacuum and the evaporation rapidly cools the liquid to temperatures as low as 210 K.[35] The small jet diameter and lower temperatures allow for the use of vacuum based photoemission and x-ray spectroscopies to explore the structure of water and aqueous solution at the liquid surface.[36–38] For example, Nilsson *et al.* have used a liquid jet to generate micron-size supercooled liquid water droplets as low as 227 K.[39] Another technique uses the supersonic expansion of water vapor to achieve cooling rates of 10^6 K/s.[40] Wyslouzil *et al.* have used this approach to measure the homogeneous ice nucleation rate between 202 and 215 K for nanometer size droplets (~13 nm).[41–43] A completely different direction has been to study the properties of water in confined spaces and on biological surfaces to inhibit crystallization.[44–46]

While these and other approaches are promising, more experimental data are needed to understand the properties of supercooled liquid water and to address many of its controversies.[29,30,47,48] We have developed a pulsed laser-heating method that will allow us to investigate deeply supercooled liquid water by producing transiently heated films, which become liquids that last for approximately 10 ns per laser pulse. Subsequent rapid cooling due to the dissipation of the heat pulse into the metal substrate effectively quenches the liquid dynamics until the next laser heating pulse arrives. The rapid heating and cooling allows the system to reach previously unattainable supercooled liquid temperatures and return to the amorphous state before significant crystallization can occur. The nanosecond time scale is long enough for many dynamical processes of interest to be investigated. For example, for diffusivities from 10^{-6} to 10^{-12} cm^2/s, the time for a molecule to diffuse 1 nm varies from 10^{-8} s to 10^{-2} s. For a 10 ns duration pulse, these times range from a single heat pulse up to 10^6 laser pulses, respectively. Thus, in this case, experiments lasting a day or less should cover most of the range of interest. Similar estimates suggest that the nucleation and growth rates for crystalline ice in the deeply supercooled region can also be studied with such transiently heated thin films.

Here, we discuss the design, implementation, and characterization of a nanosecond pulsed laser heating system for investigating nanoscale water and supercooled water films in UHV. As described below, an important goal is to achieve uniform heating across the adsorbed films, which requires a laterally homogeneous laser pulse. A second critical challenge is to accurately characterize the temperature as a function of time and position, $T(\vec{x},t)$, within the transiently heated adsorbate layer and the metal substrate. Initial experiments with the apparatus demonstrate that crystalline ice films initially held at 90 K can be rapidly transformed into liquid water films with T > 273 K. These films do not significantly recrystallize during the time they rapidly cool back to the starting temperature. Conversely, ASW films that are heated into the supercooled regime, crystallize and the crystallization kinetics can be studied versus the number of laser pulses. We recently published a preliminary report on the melting and wetting of thin ice films on Pt(111) using this nanosecond pulsed laser heating system.[49] Here, we present a more detailed description of the technique and a number of proof-of-principle studies demonstrating its utility and applicability to the study of nanoscale films of liquid water and supercooled water.

The outline for the rest of the paper is as follows: Section II presents an overview of the design considerations and heat transfer calculations of the transiently heated nanoscale films deposited on a Pt(111) substrate. A detailed description of the experimental setup is given in Section III. Section IV discusses calibration of the temperature of transiently heated thin water films, tests of the lateral homogeneity of the heating, and presents some preliminary results demonstrating the capabilities of the system.

II. DESIGN CONSIDERATIONS AND HEAT TRANSFER CALCULATIONS FOR TRANSIENTLY HEATED NANOSCALE FILMS

Figure 1 displays a schematic overview of our approach for investigating the chemical kinetics and dynamics of transiently heated nanoscale molecular films adsorbed on a metal substrate. A key aspect of our approach is the creation of compositionally tailored, molecular films with sub-nanometer precision at low temperature on a well-characterized Pt(111) single crystal in UHV (Fig. 1(a)). After film growth, a nanosecond Nd:YAG laser is used to transiently heat the metal substrate (Fig. 1(b)). Efficient heat transfer to the adsorbed film heats them by hundreds of degrees on a nanosecond time scale to create nanoscale liquids in UHV (Fig. 1(c)). Subsequent rapid cooling, also on a nanosecond time scale, quenches the system so that a post-pulse analysis can be conducted using the tools of UHV surface science (Fig. 1(d)). For temperature jumps of ~100–200 K, peak heating and cooling rates of $\sim 1 \times 10^{10}$ K/s are achieved.

In the Introduction, several problems in chemical physics were discussed where the relevant time scales range from tens of nanoseconds to perhaps one hundred microseconds. As we show below, the lower end of this range is commensurate with the transient heating achievable with a single nanosecond

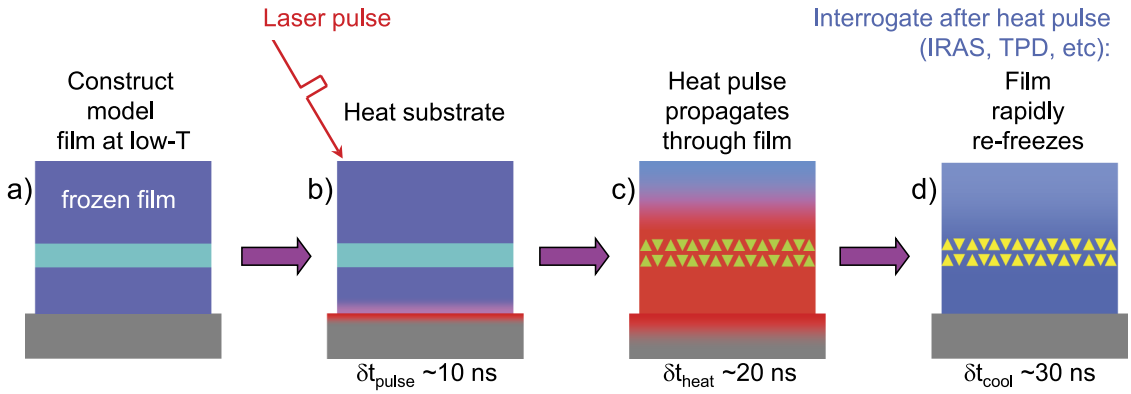

FIG. 1. Schematic of laser-induced heating and rapid cooling of an adsorbate layer on a metal substrate. (a) Compositionally tailored thin films are grown on a cold substrate (e.g., T < 120 K) using molecular beams with an isotopically or chemically distinct layer (light green). (b) A laser pulse (or pulses) from a Nd:YAG laser heats the metal substrate (e.g., Pt(111)). (c) The heat pulse rapidly propagates through the adsorbate layer and into the bulk of the metal crystal. The heat pulse may initiate physical or chemical changes in the region of interest (green triangles). (d) Diffusion of heat into the metal substrate leads to rapid cooling of adsorbate layer. The system is quenched at low temperatures and can then be interrogated with surface science techniques such as IRAS and TPD.

Nd:YAG laser pulse and longer times can be explored by increasing the number of heating pulses. Therefore, it will be useful to begin with some general considerations and "back-of-the-envelope" estimates of various quantities for a nanoscale film adsorbed on a metal substrate that is heated with a nanosecond laser pulse. Initially, we will ignore the temperature dependence of the physical properties (e.g., specific heat capacity, thermal conductivity, etc.) of the metal substrate and the adsorbate layer. However, these dependencies are included in the numerical simulations described below. The first point to note is that with relatively low-power, nanosecond laser pulses, the electron and phonon temperatures remain in equilibrium at all times. As a result, two-temperature models (or their equivalent), which have been developed to treat the heating accompanying high-power pico- and femto-second laser pulses,[50–52] are not required in this case.

For the experiments reported here, the adsorbed films do not absorb the laser beam that is used to produce the heat pulse. Instead, the metal substrate is heated by the laser and the energy subsequently diffuses into both the adsorbed film and also deeper into the metal. The absorption depth of the laser pulse in the substrate is given by the optical properties of the metal at the frequency of the incident light. For a good conductor, the penetration depth (or skin depth), χ, is given by $\chi = \sqrt{2/(\sigma\mu\omega)}$ where σ is the conductivity, μ is the magnetic permeability, and ω is the angular frequency of the radiation ($\omega = 2\pi c/\lambda$).[53] For a Nd:YAG laser pulse (λ = 1064 nm) incident on a platinum crystal, the penetration depths are ~5–10 nm at temperatures ranging from 100 to 300 K. In contrast, the Lambert absorption coefficient for 1060 nm light in water is ~0.12 cm^{-1} (corresponding to a penetration depth of ~8×10^7 nm).[54]

The penetration depth of the light is small compared to the typical distance the heat diffuses into the metal substrate, l_p, during a single laser pulse. This distance can be estimated as $l_p \sim \sqrt{\alpha^2 \tau_{laser}}$, where τ_{laser} is the duration of the laser pulse and α^2 is the coefficient of thermal diffusivity for the metal. The value of α^2 is related to its thermal conductivity, κ, density, ρ, and specific heat capacity, C_p, by $\alpha^2 = \kappa/\rho C_p$. Using the appropriate values for platinum at ~300 K (see Ref. 55) and assuming $\tau_{laser} \sim 10^{-8}$ s gives $\alpha^2 = 2.5 \times 10^{-5}$ m^2/s and $l_p \sim 500$ nm. Thus, the diffusion of heat into the substrate during the laser pulse is significant. On the other hand, our platinum crystal is 1 mm thick and the time scale for the heat pulse to diffuse throughout the crystal is approximately 40 ms. Therefore, it is sufficient to consider the heat flow within the platinum crystal and the adsorbed film without considering the heat flow through the rest of the cryostat. In the experiments, we strive to make the laser beam uniform over the entire area of the adsorbed films, which are 6.5 mm in diameter. Since l_p is small compared to the length scale for lateral variations in the laser power, we can ignore lateral heat transfer and treat the heat diffusion versus the distance normal to the surface as a one-dimensional problem. At any given lateral position across the film, the local $T(z,t)$ will be determined by the local laser energy per unit area at that spot.

Typical experiments will require temperature jumps, ΔT, in the range of 100–200 K. The absorbed energy per pulse that is required to heat the metal substrate by this amount is $\Delta E_{metal} \sim mC_p\Delta T = \rho A l_p C_p \Delta T$, where m is the mass to be heated, $m \sim \rho A l_p$, A is the area heated by the pulse, and ρ is the mass density of platinum. The crystals have $A \sim 10^{-4}$ m^2 so for $l_p \sim 5 \times 10^{-7}$ m and $\Delta T = 200$ K, $\Delta E_{metal} \sim 30$ mJ. In many cases, the energy required to heat the adsorbed film, ΔE_{film}, will be considerably less than ΔE_{metal}. For example, the amount of energy required to raise the temperature of a 100 ML thick film of water ice by 200 K is only ~1.2 mJ (using the specific heat capacity of ice at 253 K).[56] In many experiments, the vapor pressures of the adsorbed films are such that appreciable desorption can occur during a single laser pulse. However, the energy lost from the film due to desorption is a negligible fraction of the total energy absorbed. For example, using the heat transfer model described below, the calculated desorption per laser pulse for water ice with peak temperatures near the melting point is ~0.01 ML/pulse. For a film with $A = 10^{-4}$ m^2, and using the heat of sublimation of ice at the melting point, this amount of desorption corresponds to only ~1 μJ. Since radiative heat losses are also negligible, the vacuum interface is effectively an insulating boundary.

Given the estimates outlined above, it is suitable to model the heat transfer versus distance within the system as a one-dimensional problem. To account for the temperature-dependence of the thermal conductivities and specific heats of the metal substrate and the adsorbed film, it is convenient to model the system as a series of coupled ordinary differential equations (ODEs).[57] Each ODE represents a layer of some thickness, Δz_i, located at a height z_i within the adsorbed film or the metal substrate. Fourier's law of heat conduction is used to calculate the energy flowing across the boundary between two layers using the average temperature-dependent thermal conductivity of the two adjacent layers. For the layer at the vacuum interface, no heat is lost through that interface. We also choose the total thickness of our simulated metal substrate to be large enough that the temperature rise in the last layer (in the "bulk") is negligible on the time scale of interest. In that case, we can also impose an insulating boundary condition there with negligible impact on the calculated $T(z,t)$ within the film.

Laser energy is added to the metal substrate taking into account the spatial and temporal profiles of the light's absorption within the metal. Experimentally, the laser's temporal profile is measured using a photodiode and is approximately Gaussian (for improved fitting, two or more Gaussians can also be used) and the intensity decays exponentially with distance into the metal. The temperature change within any layer is calculated using the net energy flow into it, the temperature-dependent specific heat, $C_p(T)$, and the density ρ. An ODE solver is used to calculate the temperature versus time, $T(z_i,t)$, for all the layers.

The black line in Figure 2 shows $T(t)$ at the surface of a platinum crystal (without an adsorbed film) calculated using the procedure described above. The dashed purple line shows the laser energy, E_p, versus time (arbitrarily scaled). The laser pulse profile was chosen to match the temporal profile of our Nd:YAG laser (described below) as measured with a photodiode. In this example, the initial temperature was 90 K and the maximum temperature was 270 K. Maximum heating rates and cooling rates for this simulation were 2×10^{10} K/s and 5×10^{9} K/s, respectively. The peak temperature at the surface occurs approximately 4 ns after the peak laser power and occurs when the loss of energy due the diffusion of heat into the Pt substrate just matches the energy absorbed from the laser. The red line figure in Figure 2 shows the expected desorption rate versus time for a crystalline ice film at these temperatures. Since the desorption rate increases rapidly with temperature, it is sharply peaked around the maximum temperature: the full width at half maximum (FWHM) of the desorption curve is only 4.6 ns, compared to 10.3 ns for the laser pulse and 32 ns for $T(t)$. For the heat pulse shown in Figure 2, the integrated desorption over one pulse is 0.0088 monolayers (MLs). (Water coverages, in monolayers, are defined relative to the first layer of H_2O on Pt (111) as determined by the water TPD spectra—1 ML $\sim 1 \times 10^{19}$ molecules/m^2). Since many of the physical properties of interest are rapidly increasing functions of temperature, the narrowing (in time) of their temporal evolution relative to the temperature profile is an important characteristic of these transiently heated systems.

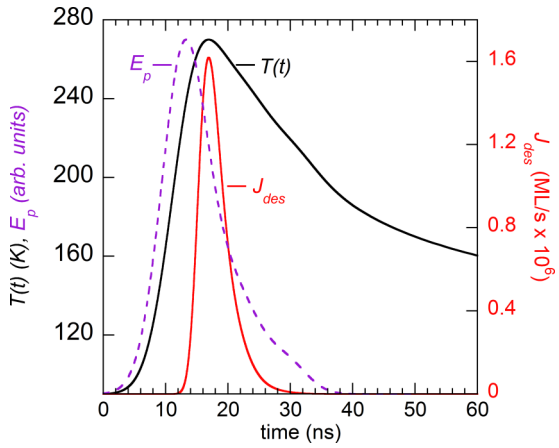

FIG. 2. Calculated temperature ($T(t)$, black line) and water desorption rate (J_{des}, red line) for an input laser pulse profile (E_p, purple line) versus time. The initial temperature was 90 K and the peak temperature was 270 K. Due to the exponential dependence of the water desorption rate on the temperature, the desorption is sharply peaked around the time of the maximum temperature.

III. EXPERIMENTAL SETUP FOR NANOSECOND PULSED LASER HEATING

A schematic for the experimental setup is shown in Fig. 3. The main components are a 10 Hz ns Nd:YAG laser (Fig. 3(a), Continuum, Powerlite DLS 8000), laser beam optics (Figs. 3(b)-3(j)), and a UHV surface science instrument (Figs. 3(k)-3(o)). The laser and beam optics are designed to deliver a laterally homogeneous, variable energy laser pulse whose temporal profile does not depend on the pulse energy. The fundamental frequency of the Nd:YAG laser (1064 nm) is used for the pulsed heating. To optimize the laser beam's spatial profile and stability, the laser is run at full power. To produce a pulse with variable energy, a variable attenuator (Fig. 3(c), Eksma Optics, model 990-0070-1064) consisting of one half-wave plate and two parallel thin film Brewster-type plate polarizers is used for tuning the beam power in the range of 0.5%–99.0% without changing the beam's spatial or temporal profile. The variable attenuator works best with a highly polarized beam, so a Brewster-angle thin film plate polarizer (Fig. 3(b)) is placed before the attenuator. A shutter (Fig. 3(e), Uniblitz T132) is employed (as necessary) to reduce the frequency of the laser pulses entering the vacuum chamber. For experiments requiring relatively few heat pulses, the pulse rate is typically set to 1 Hz.

While an ideal laser pulse for our application would have a "top-hat" spatial profile (i.e., no lateral variations), the output of a typical Nd:YAG laser, including the one used here, does not have such a profile. To overcome this problem, a custom-designed, off-axis diffractive optical element (DOE) (Fig. 3(h), Silios Technologies) was used. Other optical elements include a 2× beam expanding telescope (Figs. 3(f) and 3(g)), a focusing lens (Fig. 3(i)), and 5 steering mirrors (Fig. 3(j)). The laser beam was incident on the Pt(111) sample (Fig. 3(k))

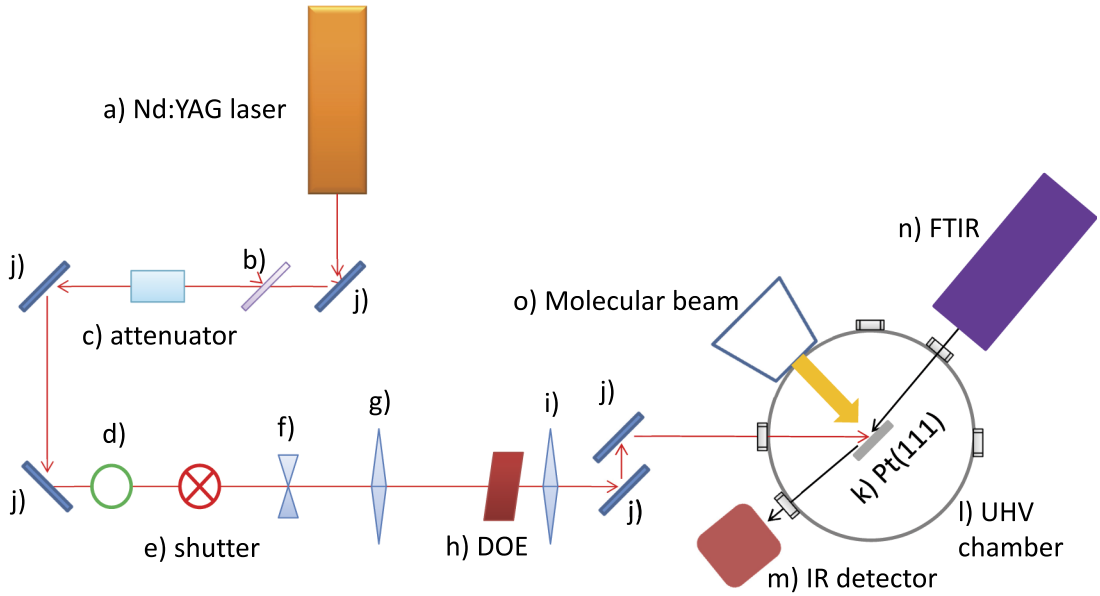

FIG. 3. Schematic of the laser, optics, and UHV chamber (top view). The optical elements include a Nd:YAG laser (a), a polarizer (b), a beam attenuator (c), an iris (d), a shutter (e), a beam expanding telescope (f) and (g), a diffractive optical element (h), a focusing lens ((i), f = 75 cm), and 5 IR mirrors (j). The optical system is interfaced with a UHV vacuum chamber (l) that has a Pt(111) single crystal (k), a molecular beam dosing system (o), an FTIR spectrometer (n), and an external IR detector (m). A variety of other surface science instrumentation on the UHV chamber is not shown in the diagram.

at an angle of 40° with respect to the surface normal. Figure 4 shows the beam profile captured with a CCD camera. At the sample position, the laser beam is ~15 mm in diameter. Because the molecular beam dosing system produces an adsorbed film with a diameter of 6.5 mm (Fig. 4, red circle), the entire adsorbate layer and the Pt(111) crystal face are contained within the flat-top region of the laser spot. With this system, p-polarized laser beam was obtained that provides laterally homogeneous heating, with repetition frequencies up to 10 Hz and in the energy range of 0–600 mJ/pulse. The system can heat the Pt(111) surface to temperatures as high as ~400 K.

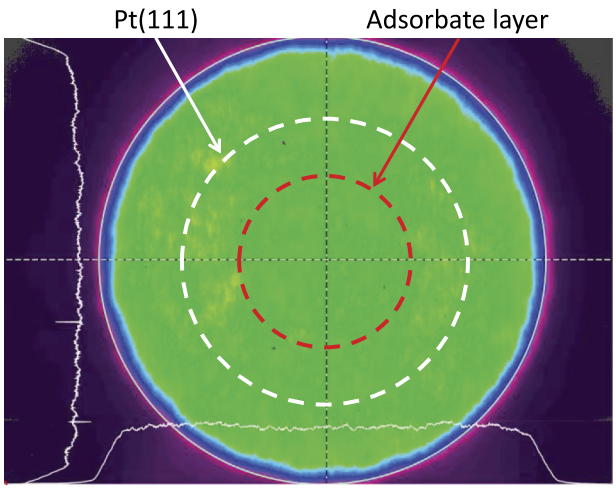

FIG. 4. CCD image of the top-hat laser beam produced by the nanosecond pulsed laser and associated optics. The image is the average of 500 laser shots. The relative size of the Pt(111) sample (10 mm) and the adsorbate layers deposited on the sample with the molecular beam dosing system (6.5 mm) are indicated by white and red circles, respectively.

The UHV system has been described in detail previously,[58,59] so only a brief description is given here. The UHV system consists of a small molecular beam source, a Pt(111) sample (Princeton Scientific, Corp.), a quadrupole mass spectrometer (QMS) (Extrel–Merlin 3500), and a Fourier transform infrared spectrometer (FTIR) (Bruker–Vertex 70). For (non-pulsed heating) temperature control, the Pt(111) substrate is resistively heated by passing current through the tantalum wire to which the Pt(111) sample is spot-welded and cooled by a closed-cycle He cryostat (Advance Research Systems–CSW 204B). The sample temperature is monitored by a K-type thermocouple spot-welded to the back side of the Pt(111) crystal. The sample is routinely cleaned by neon ion sputtering (2 keV) followed by two-minute annealing in vacuum at 950 K. The infrared beam is incident on the Pt (111) surface at grazing incidence (~84° relative to normal) and detected in the specular direction. The dosing rate for H_2O is about 0.2 ML/s, the typical temperature ramp rate for TPD is 1 K/s, and the typical base pressure for the main chamber is 8×10^{-11} Torr.

The initial phase of the nanoscale film (amorphous or crystalline) deposited on the Pt(111) is controlled by the dosing temperature. Crystalline ice films are typically grown at ~140–150 K and ASW films grow for T ≤ 120 K. After film preparation, the temperature is set and held to some initial temperature, T_0, which serves as the starting temperature for the pulsed laser heating measurements. Since thin water films, which are the subject of our initial experiments, are essentially transparent to photons with a wavelength of 1064 nm, the platinum substrate is heated first, and the water film temperature increases via heat transfer from the metal. Desorbed molecules are monitored with the QMS during the pulsed laser heating process. The QMS does not have a line-of-sight from the sample to the ionizer. Instead, a

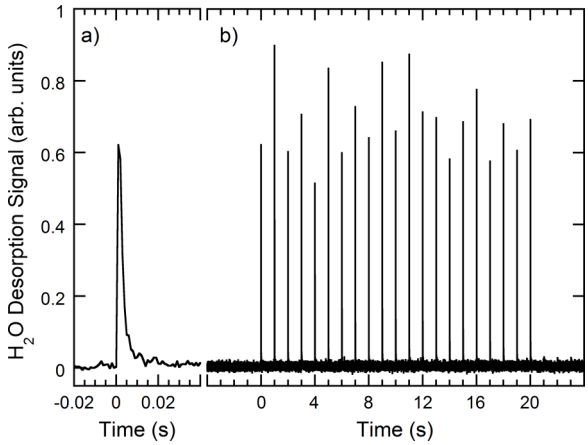

FIG. 5. H_2O desorption versus time for a 150 ML CI film with $T_0 = 90$ K that was heated to 270 K with laser pulses at 1 Hz. (a) An expanded view of the first pulse in the series. (b) The variation in the pulse height is due to a combination of variation in the laser pulse energy and the precise timing of the desorption pulse relative to the 1 ms bin width for data acquisition.

subset of the atoms or molecules desorbing from the surface enter a 1.7 cm diameter stainless steel tube positioned near the sample that leads to the ionizer of the QMS. The tube, which acts as an integrating cup for the QMS,[60] also broadens the initially narrow pulse of desorbing molecules such that they are detected over ~0.01 s. Figure 5 shows an example of the H_2O desorption versus time measured with the QMS for a 150 ML crystalline ice film that was held at a starting temperature of 90 K and heated to 270 K (see below) at 1 Hz. We will refer to desorption measured in this way as the pulsed-heating desorption or PHD. The integral of each individual pulse versus time (see, e.g., Fig. 5(a)) is proportional to the desorption yield per pulse. For the data shown in Figure 5, the pulse-to-pulse to variation of the integrated PHD signal is ±12%, which corresponds to a variation of ±1.5 K in temperature and ±1% in the laser pulse energy.

IRAS spectra can be taken before and after pulsed laser heating to investigate changes in the adsorbate layers, such as phase transitions,[61–65] isotopic mixing,[28,62] and diffusion.[26,29] TPD of weakly bound gases (e.g., rare gases and N_2) is also used to investigate changes in the transiently heated films.[9,11] The TPD spectra of the adsorbate layers after pulsed heating also provides valuable information on the chemical and physical processes occurring in the films.

IV. TEMPERATURE CALIBRATION OF TRANSIENTLY HEATED FILMS

Two of the primary challenges with transiently heated nanoscale films are achieving a laser pulse that is uniform over the area of the adsorbed film and characterizing the temperature versus time and position, $T(z,t)$, within the films. In this section, we describe experiments that have been done to characterize these properties for the experimental setup described in Section III. To characterize the temporal characteristics of the heat pulse, we have measured the reflectivity of the transiently heated Pt(111). In addition, we have used measurements of the laser-induced desorption of thin water films to characterize maximum temperatures obtained versus the laser pulse energy, and the lateral homogeneity of the laser pulses.

A. Transient reflectivity of laser-heated Pt(111)

The reflectivity of metals depends on their temperature[66] and thus provides a method to characterize $T(t)$ at the surface of the transiently heated substrate.[67–70] Figure 6 shows the change in the reflectivity, $\Delta R(t) = R(T(t))/R_0$, versus time when the Pt(111) sample was heated with 400 mJ pulses (red line), where $R(T)$ is the reflectivity of the platinum at temperature, T, and $R_0 = R(T_0)$ where T_0 is the initial temperature. For this experiment, the intensity of a red diode laser (630 nm) reflected off the sample was measured versus time with a photodiode while the sample was irradiated with the IR pulses from the Nd:YAG laser. Based on experiments described below, the maximum temperature achieved during the laser pulses was 297 K. As expected, the change in reflectivity is small and negative.[66,67,70] The reflectivity decreases quickly as the sample heats up and recovers more slowly as the sample cools down. The FWHM of the dip in reflectivity is ~25 ns.

The change in reflectivity with temperature can be approximately linear or have some curvature, depending on the metal.[66] Previous experiments indicate that for platinum, the thermoreflectance coefficient, which is a measure of dR/dT, varies approximately linearly with temperature for 290 K < T ≤ 600 K for both 470 nm and 530 nm light.[70] Therefore, $\Delta R(t)$ should be approximately quadratic in $T(t)$: $\Delta R(t) = 1 - (\alpha/R_0)(T(t) - T_0) - (\beta/R_0)(T(t) - T_0)^2$. Assuming this, same functional form applies for 630 nm light for 90 K ≤ T ≤ 300 K and using $\alpha/R_0 = 1.9 \times 10^{-5}$ K^{-1}

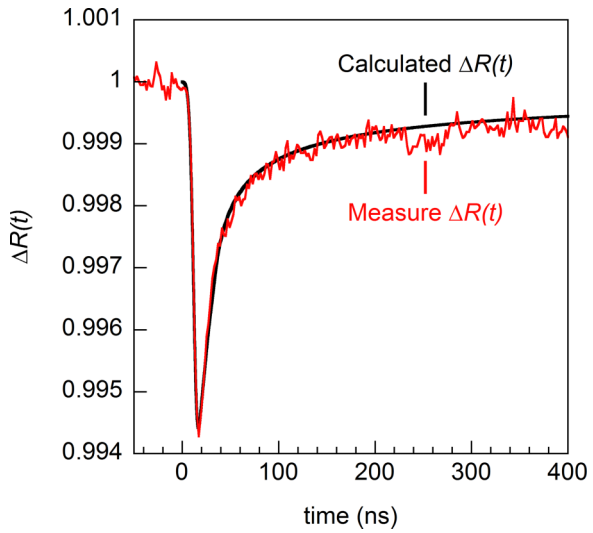

FIG. 6. Measured and calculated change in reflectivity versus time during pulsed heating. The Pt(111) crystal, with an initial temperature of 90 K, was heated with 400 mJ IR pulses at 10 Hz and the change in the reflected intensity of a diode laser, $\Delta R(t)$, was measured versus time, red line. Note that the maximum reflectivity change is small and the measurement is the average of 1.2×10^4 pulses. Using $T(t)$ calculated with the heat transfer model (see Fig. 2, black line) and the temperature-dependent reflectivity of the platinum substrate, the change in reflectivity was calculated (black line). The calculated reflectivity matches the measured value.

and $\beta/R_0 = 4.0 \times 10^{-8}$ K^{-2}, we calculated $\Delta R(t)$ using $T(t)$ calculated with the heat transfer model (Figure 6, black line). As seen in the figure, the calculated reflectivity versus time captures the important features of the measurement. In particular, the quick increase in temperature and subsequent rapid cooling leads to the initial rapid drop in the reflectivity and its recovery to ~0.998 after only ~50 ns. The slow increase in reflectivity at longer times occurs as the heat diffuses further into the crystal and the temperature at the surface returns to the initial temperature. (At ~300 ns, the calculations indicate that the heat pulse has diffused approximately 15 μm into the substrate). The close agreement between the measured and calculated $\Delta R(t)$ indicates that the heat transfer model correctly describes $T(t)$ for the transiently heated sample.

B. Desorption per pulse versus laser energy per pulse

In this section, we describe a method to calibrate the temperature using the measured desorption per pulse from a transiently heated adlayer as a function of the energy per pulse, E_p, of the laser. Because the vapor pressure of a water adlayer increases dramatically (roughly Arrhenius-like) with temperature, the desorption per laser pulse is quite sensitive to the temperature. The desorption flux for crystalline ice, $J_{des}(T)$, can be calculated from the known temperature-dependent vapor pressure of ice, $P_{ice}(T)$: $J_{des}(T) = \frac{P_{ice}(T)}{\sqrt{2\pi m k_b T}}$, where m is the mass of water and k_b is Boltzmann's constant.[71] (An equivalent expression applies for liquid water). Using $T(t)$ calculated with the heat transfer model (e.g., Fig. 2), the integral of $J_{des}(T(t))$ over a single pulse gives the desorption per pulse, $\tilde{J}_{des}(T_{\max}) = \int J_{des}(T(t))dt$, where T_{max} is the maximum temperature obtained during the pulse. We use T_{max} as a characteristic to designate a particular $T(t)$ for the transient-heating experiments. The calculation can be repeated for a variety of different heat pulses covering a range of maximum temperatures to create a table of T_{max} versus $\tilde{J}_{des}(T_{\max})$. Measurements of $\tilde{J}_{des}(T_{\max})$ are then used to determine the corresponding $T(t)$ for a given laser pulse energy.

Figure 7(a) shows $\tilde{J}_{des}(T_{\max})$ versus E_p for 10 ML ASW and CI films. For these experiments, the desorption from the water film was measured three ways: (a) from comparisons of the integrated intensity of the water TPDs with and without pulsed heating (Fig. 7(a), green diamonds), (b) via the integrated intensity of the OH-stretch region in IRAS (Fig. 7(a), red squares), and (c) from the magnitude of the integrated water PHD (Fig. 7(a), open black circles). In IRAS, the integrated OH intensity decreases linearly versus the number of laser pulses (data not shown) and the slope of this line is $\tilde{J}_{des}(T_{\max})$. For the PHD, the integrated signal is proportional to the desorption yield per pulse. As E_p is varied from 250 mJ/pulse to 455 mJ/pulse, the desorption rate varies by over three orders of magnitude, and as seen in Figure 7(a), the three techniques for measuring $\tilde{J}_{des}(T_{\max})$ are all consistent. For the data shown in Figure 7(a), the desorbing molecules undergo fewer than 1 gas-phase collision (on average) above the surface due to the relatively low desorption fluxes and the short duration of the heat pulses.[72]

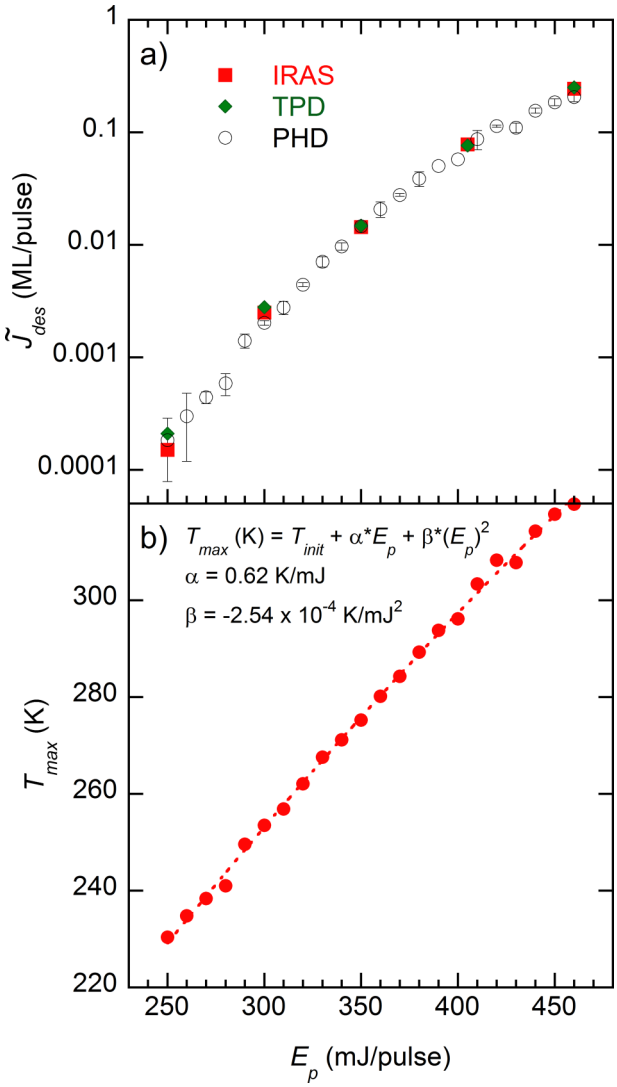

FIG. 7. (a) The experimental desorption per pulse, J_{des}, versus laser pulse energy of 10 ML CI or ASW films determined from IRAS (red squares), water TPD (green diamonds), and water PHD (black circles). The error bars for the PHD data indicate the standard deviation obtained from repeated measurements at the same pulse energy. (b) Maximum temperature, T_{max}, versus the laser pulse energy. J_{des} at each laser power (from a) was converted to a maximum temperature, $T_{max}(E_p)$, using the calculated $T(t)$. Thus, for any given laser pulse energy, the corresponding $T(t)$ can be calculated, providing a temperature calibration.

As described above, each measured desorption per pulse corresponds to a particular temperature as a function of time, $T(t)$, and its corresponding T_{max} for the transiently heated film. Figure 7(b) (red circles) shows T_{max}, obtained from the measured desorption rates, versus E_p. This data can be fit with a second order polynomial, providing a temperature calibration for the transiently heated films.

C. Lateral homogeneity of the laser-induced heating

To characterize the lateral homogeneity of the laser heating and the resulting temperatures that are obtained, we investigated lateral variations in the desorption rate of transiently heated thin water films. The basic idea is to adsorb water films and then measure the area of the underlying

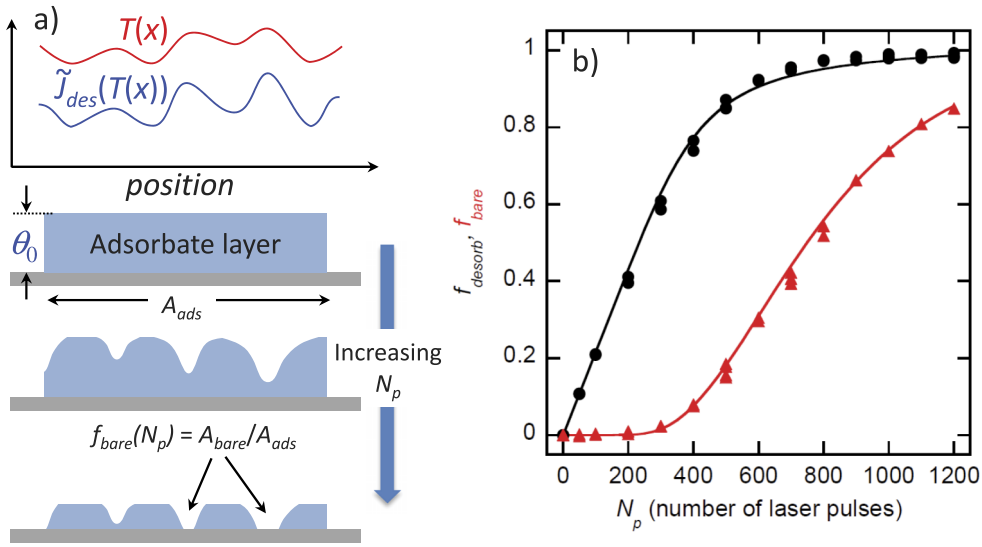

FIG. 8. (a) Schematic of the desorption profile that occurs when a laterally inhomogeneous laser pulse is used to heat an adsorbate layer. Small variations in the lateral temperature, $T(x)$ (top, red line), lead to larger variations in the desorption rate for the adsorbate layer (top, blue line). The lateral variations in the desorption rate cause the hotter portions of the adsorbate layer to completely desorb earlier than the colder regions, exposing the underlying Pt substrate. (b) The fractional area of the bare substrate, f_{bare} (red triangles), the fraction of the water desorbed, f_{desorb} (black circles) versus the number of laser pulses, N_p. Using a model that assumes a Gaussian distribution of temperatures across the sample, calculated values for f_{bare} (red line) and f_{desorb} (black line) reproduce the experimental results.

Pt(111) substrate that is exposed by the desorbing water films versus the number of heating pulses (see Figure 8(a)). Since water desorbs faster from the hotter areas, the substrate will be uncovered at earlier times in those regions, providing information on the homogeneity of the heating. As described above, the temperature, averaged over the adsorbate layer, can also be calculated from the measured desorption rate per laser pulse of the adsorbate layer. As described in earlier publications,[9–11] we use rare gas adsorption/desorption to measure the amount of the surface that is not covered with any water, covered with 1 monolayer, or multilayers of water.

As an example of this approach, Figure 8(b) shows the results of an experiment for a 10 ML ASW film irradiated with 360 mJ laser pulses with T_0 = 90 K. Using the temperature calibration shown in Figure 7(b), T_{max} = 280 K. The fraction of the initially covered Pt(111) surface exposed as the water film desorbs, f_{bare} (red triangles), and the fraction of the water that has desorbed, f_{desorb} (black circles), are shown versus the number of laser pulses, N_p (see Figure 8(b)). f_{desorb} was determined using the integrated intensity of the water OH stretch region in IRAS, $f_{desorb}(N_p) = 1 - \frac{IRAS(N_p)}{IRAS(N_p=0)}$, where $IRAS(N_p)$ is the integrated water signal after N_p laser pulses. For $N_p <\sim 300$, there are no bare spots in the water film, $f_{bare} \sim 0$, and f_{desorb} increases linearly. For $N_p > 300$, the water film has completely desorbed from the hotter portions of the substrate, f_{bare} begins to increase, and—because the bare regions no longer contribute to the water desorption—$\frac{df_{desorb}}{dN_p}$ decreases. As N_p increases further, the water film completely desorbs from successively colder regions of the surface and f_{bare} continues to increase. When only the first monolayer remains in some area, the desorption rate for that area decreases further due to the fact that the adsorption energy of the monolayer is larger than that of the multilayer.

Knowing the adsorption energies of the water monolayer and multilayer films on Pt(111), a quantitative model of the desorption can be built using various assumed temperature distributions across the sample. The results of the model can then be compared to the experiments shown in Figure 8(b). For simplicity, a one dimensional model of n cells (with n = 1000, for example) representing the lateral positions of water film was constructed with various trial temperature distributions. For each cell, i, $f_{desorb}(N_p, i)$, and $f_{bare}(N_p, i)$ are calculated for the temperature of that cell, T_i. For the entire film, $f_{desorb}(N_p)$ and $f_{bare}(N_p)$ are the averages of $f_{desorb}(N_p, i)$ and $f_{bare}(N_p, i)$ over all the cells. Figure 8(b), shows $f_{bare}(N_p)$ (red line) and $f_{desorb}(N_p)$ (black line) for a model with a Gaussian probability distribution for the temperatures in the cells, $P(T_i) = \exp[-(T_i - T^*)^2/\sigma^2]$ where T^* = 278 K and σ = 5 K. It can be seen that the model reproduces the experimental results. The FWHM for the temperature distribution is ~8.3 K, corresponding to a variation of ±1.5% in the maximum local temperature. Because the starting temperature is 90 K, this temperature variation corresponds to a variation in the laser pulse energy of ±2.7% across the entire sample. As shown in Figure 4, the spatial distribution of these small variations in the laser power, and hence the temperatures, is random. Note that this temperature distribution agrees with T_{max} calculated based on the laser pulse energy and the measured desorption (280 K, see Fig. 7).

It should be noted that the temperature distribution used to model the data in Figure 8(b) is not unique, since we can also obtain similar results with other temperature distributions. However, the width of the temperature distribution, which represents the temperature variations across the film, is an important parameter. Any temperature distribution that reproduces the experiments will have a similar width as the one used for the model in Figure 8(b).

D. Proof-of-principle experiments

As discussed in the Introduction, the ability to create nanoscale liquid water and supercooled liquid water films in UHV should allow us to investigate a variety of phenomena that are of interest in chemical physics. In this section, we will present some proof-of-principle experiments that demonstrate some of these capabilities.

Most of the experiments we envision for investigating the kinetics and dynamics in liquid and supercooled liquid water films will require that these films do not crystallize appreciably during a single laser pulse. Figure 9(a) shows the IRAS spectra for a 50 ML ASW film that was grown at 90 K (black line) and after that film was heated to 305 K for 1, 3, and 100 laser pulses (red, green, and blue lines, respectively).

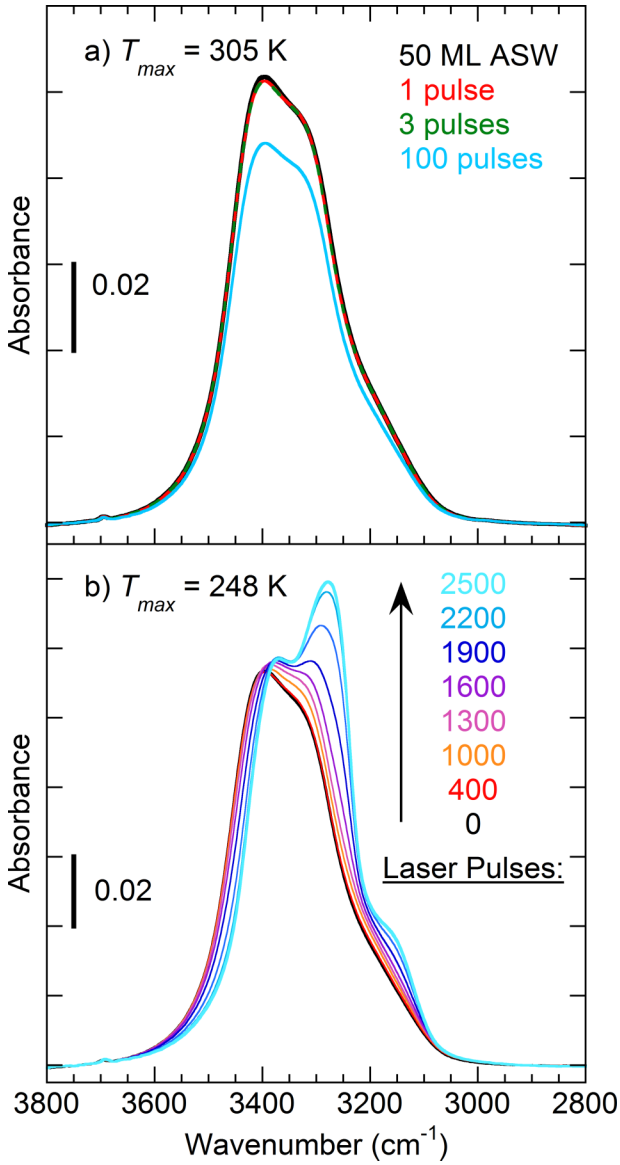

FIG. 9. IR spectra of transiently heated 50 ML water films on Pt(111). For both (a) and (b), a 50 ML ASW film was deposited at 90 K on Pt(111) (black line). The IR spectra are obtained at T = 90 K after pulsed heating. (a) For T_{max} = 305 K, aside from desorption, the IR spectra are essentially identical and characteristic of ASW. (b) For T_{max} = 248 K, as the number of heat pulses increases, the initially amorphous film crystallizes.

After 1 and 3 pulses, there is essentially no change in the spectra indicating that negligible crystallization occurs during the cooldown phase after each heat pulse. After 100 pulses, the overall intensity has decreased due to the relatively rapid desorption occurring at such high temperatures, but the IR spectrum is still consistent with an ASW film. For a 50 ML ASW film (Fig. 9(b), black line) that is heated to T_{max} = 248 K, IRAS shows that for the first ~400 laser pulses, essentially no crystallization is observed (Fig. 9(b), red line). At longer times (i.e., larger N_p), the IR spectra undergo changes characteristic of crystallization.[26,73,74] For this temperature, the crystallization is largely complete after 2500 pulses. The data shown in Figure 9(b) can be analyzed to extract the extent of crystallization versus N_p, and experiments such as these will be used to investigate the crystallization kinetics in the "no-man's-land."

For an ASW film that is transiently heated above the bulk melting point and rapidly cooled back to 90 K, the IRAS spectra before and after heating with a few pulses are essentially identical (Fig. 9(a)). In contrast, for an initially crystalline ice film that is heated above the bulk melting point, the film progressively melts as N_p increases. Figure 10(a) shows an example where a 50 ML crystalline ice film (black line, as grown) was heated to 300 K. After a single pulse (Fig. 10(a), blue line), the film shows substantial melting. However, analysis of the IR spectrum indicates that film is still approximately 50% crystalline (not shown). More heat pulses lead to increased melting and the film has completely melted for $N_p \geq 10$. These results demonstrate that the initially crystalline ice film progressively melts during the brief time it is above the melting point and does not substantially recrystallize during the subsequent cooldown. Rapid cooling of micron-sized water droplets on a cold substrate is one of the standard methods to produce ASW (also called hyperquenched glassy water).[75] The results in Figure 10(a) show that for the transiently heated films, the rapid cooling occurring at the end of the laser pulse is also sufficient to quench the liquid film into the glassy state with negligible recrystallization.

Based on energetic considerations, the heat transfer calculations discussed in Section II suggest that if there is efficient heat transfer between the metal substrate and the crystalline ice film, a film heated to 300 K should completely melt within a single heat pulse. One possible explanation for the observations is inefficient heat transfer across the water/Pt interface, corresponding to a large Kapitza resistance.[76,77] However, melting kinetics within the ice films can also play a role.[78] The melting kinetics of these transiently heated nanoscale films will be the subject of future investigations.

For a crystalline ice film that is capped with an ASW layer and heated below the bulk melting point, crystallization proceeds from the CI/ASW interface without the need for nucleating the crystalline phase. As a result, the crystallization proceeds more rapidly. Figure 10(b) shows an example where a 50 ML crystalline ice film was capped with a 50 ML ASW film (black line) and then heated to 253 K. For N_p < 100 pulses, the film rapidly crystallizes (Fig. 10(b), blue lines) and is essentially completely crystalline by N_p = 300 (Fig 10(b), red line). These results can be compared to Figure 9(b) where, in the absence of a crystalline ice template, crystallization

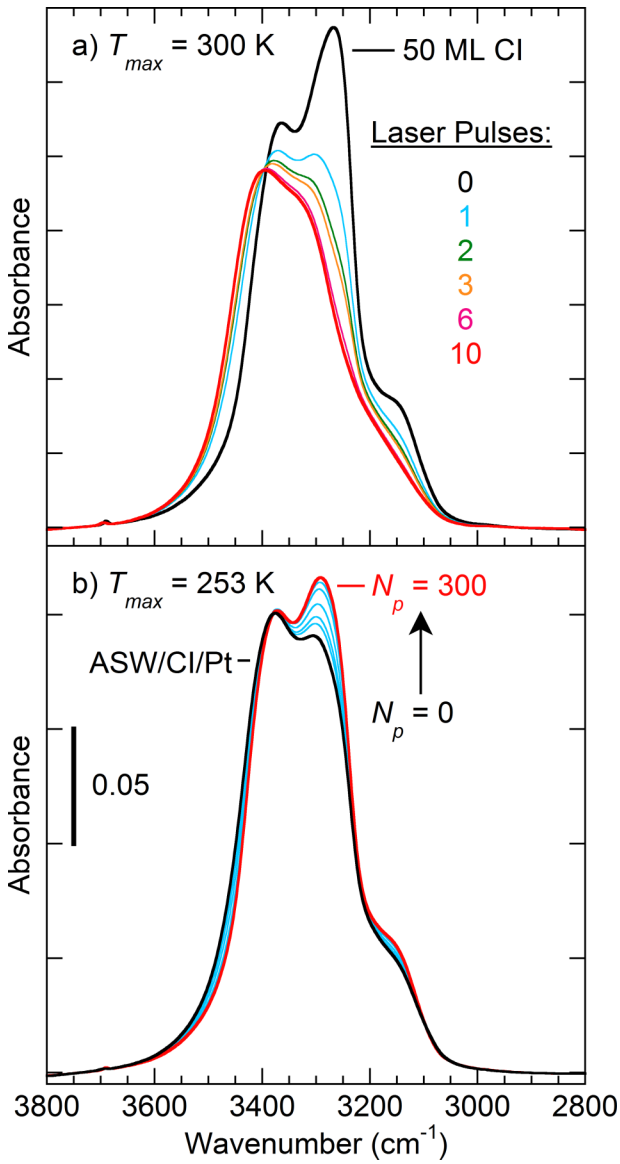

FIG. 10. (a) A 50 ML crystalline ice film (black line), which was heated to T_{max} = 300 K, partially melted after a single pulse (blue line) and completely melted for $N_P \geq 10$. (b) A 50 ML crystalline ice film that was capped with a 50 ML ASW film (black line) and heated to T_{max} = 253 K crystallized as N_P increased. The blue lines show the spectra after N_P = 15, 20, 30, 50, and 70. After 300 pulses, the film has completely crystallized (red line).

takes significantly longer. Experiments such as these will allow us to determine both the growth rate for crystalline ice and the volume nucleation rate as a function of temperature for deeply supercooled liquid water films.

V. CONCLUSION

We have developed, tested, and characterized a nanosecond pulsed laser heating system to explore the properties of supercooled liquids and liquid/solid interfaces in UHV. The system is capable of rapidly heating and cooling nanoscale films adsorbed on clean, well-characterized metal single crystals. With this system, water films deposited at cryogenic temperatures can be transiently heated to temperatures anywhere from ~100 K (or even lower) to the boiling point of liquid water—thus spanning the range from deeply supercooled water to normal liquid water—for approximately 20 ns per laser pulse. Rapid cooling after each laser pulse quenches the adsorbed films such that changes can be probed after it returns cryogenic temperatures. As a result, the time-dependent changes in the film can be studied by simply varying the number of incident laser pulses—effectively allowing the construction of a "stop-action" movie of the processes occurring at higher temperatures. Preliminary results show that initially crystalline ice films melt when heated above 273 K and quench into ASW, while ASW films heated temperatures below 273 K crystallize. We have recently used the system described here to investigate the wetting of nanoscale liquid drops on Pt(111).[49] More generally, we expect that the system described here will provide experimental data to help unravel some of the outstanding puzzles and anomalies of the chemical dynamics and kinetics of nanoscale liquids and liquid/solid interfaces.

ACKNOWLEDGMENTS

This work was supported by the US Department of Energy (DOE), Office of Science, Office of Basic Energy Sciences, Division of Chemical Sciences, Geosciences & Biosciences. Pacific Northwest National Laboratory (PNNL) is a multiprogram national laboratory operated for DOE by Battelle. The research was performed using EMSL, a national scientific user facility sponsored by the Department of Energy's Office of Biological and Environmental Research and located at Pacific Northwest National Laboratory.

[1]H. Qian and D. A. Beard, Biophys. Chem. **114**, 213 (2005).
[2]M. Gratzel, Nature **414**, 338 (2001).
[3]A. Hagfeldt and M. Gratzel, Chem. Rev. **95**, 49 (1995).
[4]B. Oregan and M. Gratzel, Nature **353**, 737 (1991).
[5]J. M. Herrmann, Catal. Today **53**, 115 (1999).
[6]A. L. Linsebigler, G. Q. Lu, and J. T. Yates, Chem. Rev. **95**, 735 (1995).
[7]T. L. Thompson and J. T. Yates, Chem. Rev. **106**, 4428 (2006).
[8]Report of the Basic Energy Sciences Workshop on Basic Research Needs for Advanced Nuclear Energy Systems, 2006.
[9]G. A. Kimmel, N. G. Petrik, Z. Dohnalek, and B. D. Kay, J. Chem. Phys. **125**, 044713 (2006).
[10]G. A. Kimmel, N. G. Petrik, Z. Dohnalek, and B. D. Kay, J. Chem. Phys. **126**, 114702 (2007).
[11]G. A. Kimmel, N. G. Petrik, Z. Dohnálek, and B. D. Kay, Phys. Rev. Lett. **95**, 166102 (2005).
[12]A. Hodgson and S. Haq, Surf. Sci. Rep. **64**, 381 (2009).
[13]G. A. Kimmel, J. Matthiesen, M. Baer, C. J. Mundy, N. G. Petrik, R. S. Smith, Z. Dohnalek, and B. D. Kay, J. Am. Chem. Soc. **131**, 12838 (2009).
[14]G. A. Kimmel, M. Baer, N. G. Petrik, J. Vande Vondele, R. Rousseau, and C. J. Mundy, J. Phys. Chem. Lett. **3**, 778 (2012).
[15]S. Nie, P. J. Feibelman, N. C. Bartelt, and K. Thurmer, Phys. Rev. Lett. **105**, 026102 (2010).
[16]A. Michaelides and K. Morgenstern, Nat. Mat. **6**, 597 (2007).
[17]J. Cerda, A. Michaelides, M. L. Bocquet, P. J. Feibelman, T. Mitsui, M. Rose, E. Fomin, and M. Salmeron, Phys. Rev. Lett. **93**, 116101 (2004).
[18]T. Mitsui, M. K. Rose, E. Fomin, D. F. Ogletree, and M. Salmeron, Science **297**, 1850 (2002).
[19]A. Verdaguer, G. M. Sacha, H. Bluhm, and M. Salmeron, Chem. Rev. **106**, 1478 (2006).
[20]G. Ketteler, S. Yamamoto, H. Bluhm, K. Andersson, D. E. Starr, D. F. Ogletree, H. Ogasawara, A. Nilsson, and M. Salmeron, J. Phys. Chem. C **111**, 8278 (2007).
[21]H. Bluhm, J. Electron Spectrosc. Relat. Phenom. **177**, 71 (2010).
[22]T. Kendelewicz, S. Kaya, J. T. Newberg, H. Bluhm, N. Mulakaluri, W. Moritz, M. Scheffler, A. Nilsson, R. Pentcheva, and G. E. Brown, Jr., J. Phys. Chem. C **117**, 2719 (2013).

[23]A. Verdaguer, C. Weis, G. Oncins, G. Ketteler, H. Bluhm, and M. Salmeron, Langmuir **23**, 9699 (2007).
[24]S. Yamamoto, K. Andersson, H. Bluhm, G. Ketteler, D. E. Starr, T. Schiros, H. Ogasawara, L. G. M. Pettersson, M. Salmeron, and A. Nilsson, J. Phys. Chem. C **111**, 7848 (2007).
[25]X. Zhang and S. Ptasinska, J. Phys. Chem. C **118**, 4259 (2014).
[26]R. S. Smith, N. G. Petrik, G. A. Kimmel, and B. D. Kay, Acc. Chem. Res. **45**, 33 (2012).
[27]P. G. Debenedetti and F. H. Stillinger, Nature **410**, 259 (2001).
[28]R. S. Smith, Z. Dohnálek, G. A. Kimmel, K. P. Stevenson, and B. D. Kay, Chem. Phys. **258**, 291 (2000).
[29]R. S. Smith and B. D. Kay, Nature **398**, 788 (1999).
[30]O. Mishima and H. E. Stanley, Nature **396**, 329 (1998).
[31]M. Chonde, M. Brindza, and V. Sadtchenko, J. Chem. Phys. **125**, 094501 (2006).
[32]V. Sadtchenko, M. Brindza, M. Chonde, B. Palmore, and R. Eom, J. Chem. Phys. **121**, 11980 (2004).
[33]E. H. G. Backus, M. L. Grecea, A. W. Kleyn, and M. Bonn, J. Phys. Chem. B **111**, 6141 (2007).
[34]O. Rebolledo-Mayoral, J. Stomberg, S. McKean, H. Reisler, and C. Wittig, J. Phys. Chem. C **116**, 563 (2012).
[35]M. Faubel, S. Schlemmer, and J. P. Toennies, Z. Phys. D **10**, 269 (1988).
[36]M. Faubel, B. Steiner, and J. P. Toennies, J. Chem. Phys. **106**, 9013 (1997).
[37]J. D. Smith, C. D. Cappa, K. R. Wilson, B. M. Messer, R. C. Cohen, and R. J. Saykally, Science **306**, 851 (2004).
[38]B. Winter and M. Faubel, Chem. Rev. **106**, 1176 (2006).
[39]H. Laksmono, T. A. McQueen, J. A. Sellberg, N. D. Loh, C. Huang, D. Schlesinger, R. G. Sierra, C. Y. Hampton, D. Nordlund, M. Beye, A. V. Martin, A. Barty, M. M. Seibert, M. Messerschmidt, G. J. Williams, S. Boutet, K. Arnann-Winkel, T. Loerting, L. G. M. Pettersson, M. J. Bogan, and A. Nilsson, J. Phys. Chem. Lett. **6**, 2826 (2015).
[40]A. Khan, C. H. Heath, U. M. Dieregsweiler, B. E. Wyslouzil, and R. Strey, J. Chem. Phys. **119**, 3138 (2003).
[41]A. Bhabhe, H. Pathak, and B. E. Wyslouzil, J. Phys. Chem. A **117**, 5472 (2013).
[42]C. H. Heath, K. A. Streletzky, B. E. Wyslouzil, J. Wolk, and R. Strey, J. Chem. Phys. **118**, 5465 (2003).
[43]A. Manka, H. Pathak, S. Tanimura, J. Woelk, R. Strey, and B. E. Wyslouzil, Phys. Chem. Chem. Phys. **14**, 4505 (2012).
[44]F. Mallamace, C. Branca, C. Corsaro, N. Leone, J. Spooren, H. E. Stanley, and S.-H. Chen, J. Phys. Chem. B **114**, 1870 (2010).
[45]F. Mallamace, M. Broccio, C. Corsaro, A. Faraone, U. Wanderlingh, L. Liu, C. Y. Mou, and S. H. Chen, J. Chem. Phys. **124**, 161102 (2006).
[46]F. Mallamace, C. Corsaro, P. Baglioni, E. Fratini, and S.-H. Chen, J. Phys.: Condens. Matter **24**, 064103 (2012).
[47]P. G. Debenedetti, J. Phys.: Condens. Matter **15**, R1669 (2003).
[48]P. G. Debenedetti and H. E. Stanley, Phys. Today **56**(6), 40 (2003).
[49]Y. Xu, C. J. Dibble, N. G. Petrik, R. S. Smith, B. D. Kay, and G. A. Kimmel, J. Phys. Chem. Lett. **7**, 541 (2016).
[50]H. E. Elsayedali, T. B. Norris, M. A. Pessot, and G. A. Mourou, Phys. Rev. Lett. **58**, 1212 (1987).
[51]T. A. Germer, J. C. Stephenson, E. J. Heilweil, and R. R. Cavanagh, J. Chem. Phys. **101**, 1704 (1994).
[52]C. K. Sun, F. Vallee, L. Acioli, E. P. Ippen, and J. G. Fujimoto, Phys. Rev. B **48**, 12365 (1993).
[53]J. D. Jackson, *Classical Electrodynamics*, 2nd ed. (John Wiley & Sons, New York, 1975).
[54]G. M. Hale and M. R. Querry, Appl. Opt. **12**, 555 (1973).
[55]*CRC Handbook of Chemistry and Physics*, 76th ed., edited by D. R. Lide (CRC Press, New York, 1995).
[56]V. F. Petrenko and R. W. Whitworth, *Physics of Ice* (Oxford University Press, Oxford, 1999).
[57]R. F. Wood and G. E. Giles, Phys. Rev. B **23**, 2923 (1981).
[58]N. G. Petrik and G. A. Kimmel, J. Chem. Phys. **121**, 3736 (2004).
[59]N. G. Petrik, R. J. Monckton, S. P. K. Koehler, and G. A. Kimmel, J. Chem. Phys. **140**, 204710 (2014).
[60]J. T. Yates, *Experimental Innovations in Surface Science: A Guide to Practical Laboratory Methods and Instruments* (Springer-Verlag New York, Inc., New York, 1998).
[61]R. S. Smith, J. Matthiesen, and B. D. Kay, J. Chem. Phys. **132**, 124502 (2010).
[62]R. S. Smith, J. Matthiesen, J. Knox, and B. D. Kay, J. Phys. Chem. A **115**, 5908 (2011).
[63]R. S. Smith, T. Zubkov, Z. Dohnalek, and B. D. Kay, J. Phys. Chem. B **113**, 4000 (2009).
[64]R. S. Smith, T. Zubkov, and B. D. Kay, J. Chem. Phys. **124**, 114710 (2006).
[65]R. J. Speedy, P. G. Debenedetti, R. S. Smith, C. Huang, and B. D. Kay, J. Chem. Phys. **105**, 240 (1996).
[66]K. Ujihara, J. Appl. Phys. **43**, 2376 (1972).
[67]C. A. Paddock and G. L. Eesley, J. Appl. Phys. **60**, 285 (1986).
[68]R. W. Schoenlein, W. Z. Lin, J. G. Fujimoto, and G. L. Eesley, Phys. Rev. Lett. **58**, 1680 (1987).
[69]R. B. Wilson, B. A. Apgar, L. W. Martin, and D. G. Cahill, Opt. Express **20**, 28829 (2012).
[70]T. Favaloro, J. H. Bahk, and A. Shakouri, Rev. Sci. Instrum. **86**, 024903 (2015).
[71]F. Reif, *Fundamentals of Statistical and Thermal Physics* (McGraw-Hill, Boston, 1965).
[72]J. P. Cowin, D. J. Auerbach, C. Becker, and L. Wharton, Surf. Sci. **78**, 545 (1978).
[73]M. S. Bergren, D. Schuh, M. G. Sceats, and S. A. Rice, J. Chem. Phys. **69**, 3477 (1978).
[74]W. Hagen, A. Tielens, and J. M. Greenberg, Chem. Phys. **56**, 367 (1981).
[75]G. P. Johari, A. Hallbrucker, and E. Mayer, Nature **330**, 552 (1987).
[76]B. H. Kim, A. Beskok, and T. Cagin, J. Chem. Phys. **129**, 174701 (2008).
[77]L. Xue, P. Keblinski, S. R. Phillpot, S. U. S. Choi, and J. A. Eastman, Int. J. Heat Mass Transfer **47**, 4277 (2004).
[78]R. F. Wood and G. A. Geist, Phys. Rev. B **34**, 2606 (1986).